Heavy-Ion Physics

Raimond Snellings

Nikhef, Science Park 105, 1098 XG Amsterdam, The Netherlands

1 Introduction

One of the fundamental questions in the field of subatomic physics is what happens to matter at extreme densities and temperatures as may have existed in the first microseconds after the big bang and exist, perhaps, in the core of dense neutron stars. The aim of heavy-ion physics is to collide nuclei at very high energies and thereby create such a state of matter in the laboratory. The experimental program started in the 1990's with collisions made available at the AGS and SPS with energies up to 20 GeV per nucleon in the center of mass, and continued at the Relativistic Heavy Ion Collider in Brookhaven, USA with energies of up to 200 GeV per nucleon. Collisions of heavy-ions at the unprecedented energy of 5.5 TeV will soon be made available at the LHC collider at CERN, Geneva, Switzerland. In these lectures I will give a brief introduction to the physics of ultra-relativistic heavy-ion collisions and review some selected highlights of the current and future experimental program. The material covered in these lectures is published in, amongst others, [1, 2, 4, 5, 6, 7, 8, 9] to which I refer the reader for more details.

2 The QCD Phase Transition and Equation of State

In the last thirty years particle physics has led to a profound understanding of the world around us, summarized in the so-called "Standard Model". It provides a coherent and precise description of the building blocks of matter and the three fundamental interactions: the weak, the strong and the electromagnetic. However, at the same time we realize that this model is far from complete. In fact we have learned that we do *not* know what most of the universe is made of. To answer the questions, what the universe is made of and how it works, is the ultimate challenge of particle physics.

In our current understanding, the universe went through a series of phase transitions after the Big Bang. These phase transitions mark the most important epochs of the expanding universe. At 10^{-11} s after the Big Bang and at a temperature $T \sim 100$ GeV ($\sim 10^{15}$ K) the electroweak phase transition took place. At this time most of the known elementary particles acquired their Higgs masses. At 10^{-5} s and at a temperature three orders of magnitude lower (170 MeV $\sim 10^{12}$ K), the strong phase transition took place. During the strong phase transition the quarks and gluons became confined in hadrons. At the same time the approximate chiral symmetry was spontaneously broken. This symmetry is crucial in the standard model and gives rise to the presence of the light pions.

The underlying theory of the strong force, QCD, is well established even though its fundamental degrees of freedom, the quarks and gluons, cannot be observed as free particles due to confinement. The known QCD Lagrangian provides in principle the complete picture but the QCD field equations are notoriously hard to solve. In fact, the two most important and interesting properties, confinement and chiral symmetry breaking, are still poorly understood from first principles.

One of the key features of QCD is that the strength of the coupling between quarks and gluons depends on their relative momenta. At higher momenta and thus smaller distances the coupling becomes weaker, leading to so called asymptotic freedom. Therefore, in a QCD system at very high temperatures the quarks and gluons are expected to become quasi-free so that the bulk properties can be described by an ideal gas Equation of State (EoS). This deconfined dense state of matter is called a Quark Gluon Plasma (QGP). Properties like energy density and pressure provide direct information about the EoS and thus about the basic degrees of freedom.

Dimensional arguments allow us to estimate the critical energy density $\epsilon_c \sim 1$ GeV/fm^3 and temperature $T_c \sim 170$ MeV. However these values imply that the transition occurs in a regime where the coupling constant is of order unity, casting doubts on results of perturbative calculations. Better understanding of the non-perturbative domain comes from lattice QCD calculations, where the field equations are solved numerically on a discrete space-time grid. Lattice QCD provides quantitative information on the QCD phase transition between confined and deconfined matter and the EoS. Figure 1a shows the calculated energy density as a function of temperature. It is seen that the energy density changes rapidly at the critical temperature $T_c \sim 170$ MeV, which is due to the rapid increase in the effective degrees of freedom. From these lattice calculations it follows that at T_c not only deconfinement sets in but that also chiral symmetry is restored. The pressure, shown in Figure 1b, changes slowly at T_c compared to the rapid increase of the energy density. Therefore the pressure gradient in the system, $\mathrm{d}P/\mathrm{d}\epsilon$, is significantly reduced during the phase transition.

In the limit of an ideal Stefan-Boltzmann gas the EoS of a QGP is given

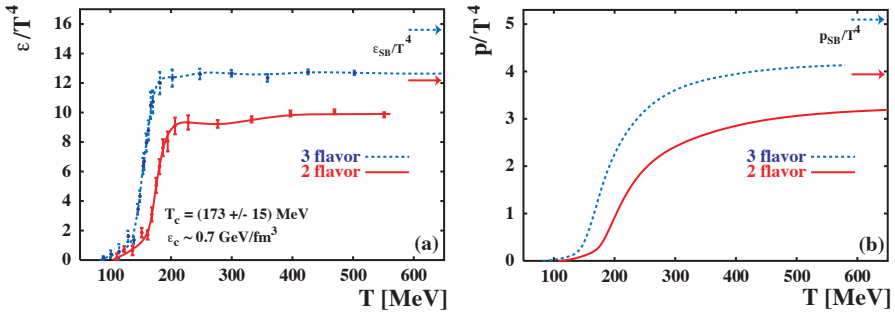

Figure 1. *a) Energy density ϵ as a function of temperature from lattice calculations. For an ideal gas the energy density is proportional to the number of thermal degrees of freedom (g). This causes the sharp increase at T_c where the system changes from approximately a pion gas, $g = 3$, into a quark gluon plasma where $g = 37$ in case of two quark flavors. The arrows in the figure indicate the ideal Stefan-Boltzmann values. b) The pressure from lattice calculations versus the temperature. The pressure also reflects the number of degrees of freedom but changes slowly at the phase boundary.*

by:

$$P_{\rm SB} = \frac{1}{3}\epsilon_{\rm SB}, \quad \epsilon_{\rm SB} = g\frac{\pi^2}{30}T^4, \tag{1}$$

$$g = n_f \times 2_s \times 2_q \times 3_c \times \frac{7}{8} + 2_s \times 8_c, \tag{2}$$

where $P_{\rm SB}$ is the pressure, $\epsilon_{\rm SB}$ the energy density and T the temperature. Each bosonic degree of freedom contributes $\frac{\pi^2}{30}T^4$ to the energy density; each fermionic degree of freedom contributes $\frac{7}{8}$ of this value. The value of g is obtained from the sum of the appropriate number of flavors $\times$ spin $\times$ quark/antiquark $\times$ color factors for the quarks and spin $\times$ color for the gluons. The energy density for a two (three) flavor QGP, where $g = 37$ ($g = 47.5$) is an order of magnitude larger than for an hadron gas where $g \sim 3$ (π^+, π^- and π^0). The corresponding Stefan-Boltzmann values of the energy density and pressure are plotted in Figure 1a and Figure 1b and show that the lattice results reach a significant fraction (0.8) of these values. The deviation from the Stefan-Boltzmann limit shows that the QCD system around T_c does *not* behave like a weakly interacting parton gas.

3 Heavy-Ion Collisions

Figure 2a shows a theoretical phase diagram of nuclear matter for two massless quarks as function of temperature and baryon chemical potential. Relativistic heavy-ion collisions are a unique tool to test this phase diagram by studying

deconfinement and the EoS of hot QCD matter under controlled conditions. Like the early universe, the hot and dense system created in a heavy-ion

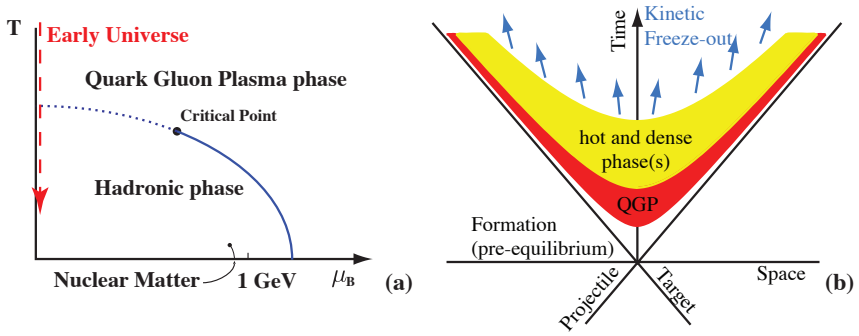

Figure 2. *a) Theoretical phase diagram of nuclear matter for two massless quarks as function of temperature T and baryon chemical potential μ_B. b) Illustration of the characteristic periods in time for a heavy-ion collision.*

collision will expand and cool down. In this time evolution the system probes a range of energy densities and temperatures, and possibly different phases. The evolution of the created system can be divided in two characteristic periods, see Figure 2b. During the formation of the system ($\leq 3\times10^{-24}$ sec) collisions with large momentum transfer occur. During this period the largest energy density is created. The system will thermalize and form the QGP provided that the quarks and gluons undergo multiple interactions. Due to the thermal pressure, the system undergoes a collective expansion and eventually becomes so dilute that it hadronizes. In the hadronic phase it further cools down via inelastic and elastic interactions until it becomes non-interacting (the freeze-out stage).

To study QCD at extreme densities ultra relativistic heavy-ion experiments have been performed at the Brookhaven Alternating Gradient Synchrotron (AGS), the CERN Super Proton Synchrotron (SPS) and the Brookhaven Relativistic Heavy Ion Collider (RHIC) with maximum center of mass energies of $\sqrt{s_{\rm NN}}$ = 4.75, 17.2 and 200 GeV respectively. The future Large Hadron Collider (LHC) will make Pb-Pb collisions available at an unprecedented energy of $\sqrt{s_{\rm NN}}$ = 5.5 TeV. Some of the main probes available in heavy-ion collisions will be described in the next section, together with a few selected results which are considered to be the highlights of the experimental program so far.

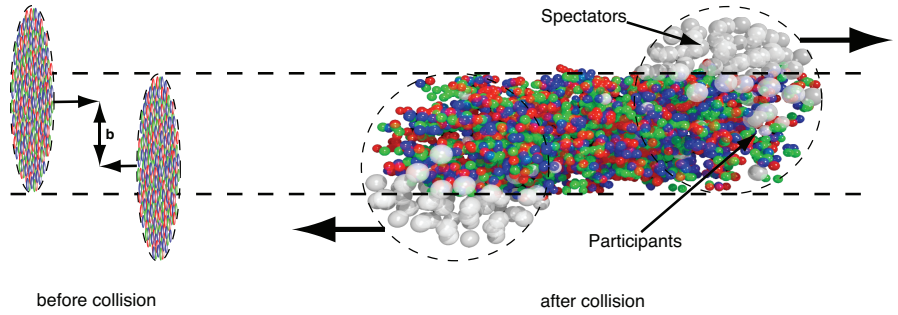

Figure 3. *Left: The two heavy-ions before collision with impact parameter* **b**. *Right: The spectators continue unaffected, while in the participant zone particle production takes place.*

3.1 Probes and observables

3.1.1 Event Characterization

Heavy ions are extended objects and the system created in a head-on collision is different from that in a peripheral collision. Therefore, collisions are categorized by their centrality. Theoretically the centrality is characterized by the impact parameter **b** (see Figure 3) which is, however, not a direct observable. Experimentally, the collision centrality can be inferred from the measured particle multiplicities if one assumes that this multiplicity is a monotonic function of **b**. Another way to determine the event centrality is to measure the energy carried by the spectator nucleons (which do not participate in the reaction) with Zero Degree Calorimetry (ZDC). A large (small) signal in the ZDC thus indicates a peripheral (central) collision.

Instead of by impact parameter, the centrality is often characterized by the so-called number of wounded nucleons or by the number of equivalent binary collisions. These measures can be related to the impact parameter **b** using a realistic description of the nuclear geometry in a Glauber calculation, see Figure 4. Phenomenologically it is found that soft particle production scales with the number of participating nucleons whereas hard processes scale with the number of binary collisions.

3.1.2 Global observables

Examples of global observables which provide important information about the created system are the particle multiplicity and the transverse energy. Figure 5 shows the transverse energy versus the collision centrality as measured at $\sqrt{s_{NN}} = 130$ GeV by the PHENIX collaboration. This measurement allows for an estimate of the energy density as proposed by Bjorken for head-on

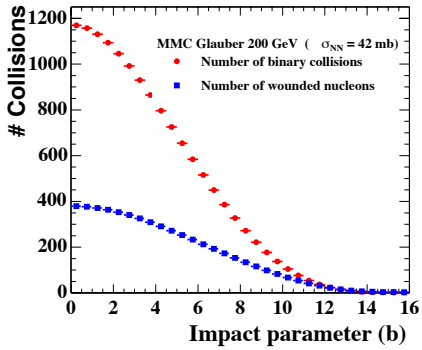

Figure 4. *Number of wounded nucleons and binary collisions versus impact parameter.*

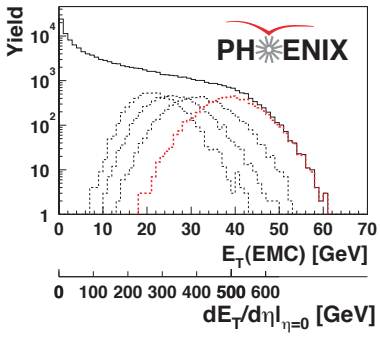

Figure 5. *Transverse energy as a function of centrality as measured by PHENIX.*

collisions

$$\epsilon = \frac{1}{\pi R^2}\frac{1}{c\tau_0}\frac{\mathrm{d}E_\mathrm{t}}{\mathrm{d}y},$$

were R is the nuclear radius and τ_0 is the effective thermalization time (0.2-1.0 fm/c). From the measured $\langle \mathrm{d}E_\mathrm{t}/\mathrm{d}\eta \rangle = 503 \pm 2$ GeV it follows that ϵ is about 5 GeV/fm^3 at RHIC. This is much larger than the critical energy density of 1 GeV/fm^3 obtained from Lattice QCD (see Figure 1).

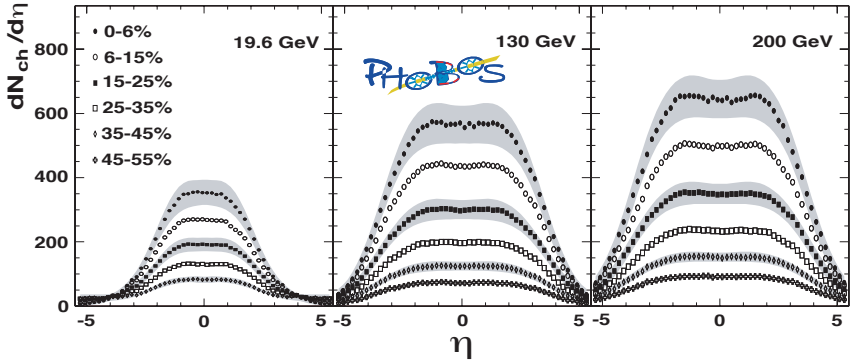

Figure 6. *Multiplicity versus pseudo-rapidity for 19.6, 130 and 200 GeV measured by PHOBOS.*

Figure 6 shows the charged particle multiplicity distributions versus the pseudorapidity η measured by PHOBOS at three different energies. Notice that in total about 5000 charged particles are produced in the most central Au+Au collisions at the top RHIC energy.

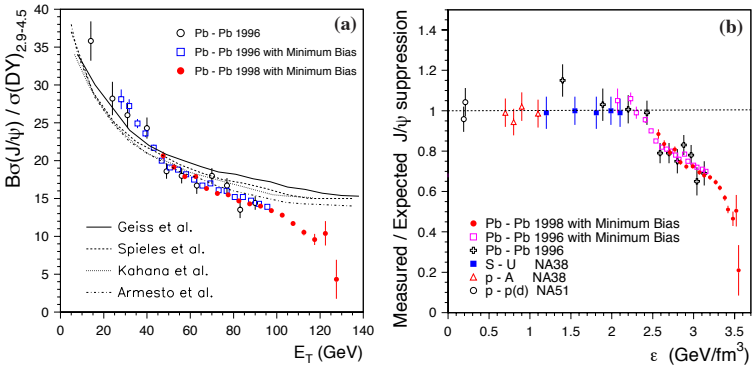

Figure 7. *a) Comparisons between the NA50 Pb-Pb measured J/Ψ data and several calculations of the suppression. b) The J/Ψ anomalous suppression as a function of the energy density reached in the collisions. Suppression is obtained from the measured cross-sections divided by the values expected from nuclear absorption. For higher energy densities an increase in the amount of suppression is observed, as can be explained by charmonium melting due to deconfinement.*

3.1.3 J/Ψ suppression

One of the most promising QGP signatures at SPS energies has been the J/Ψ suppression predicted by T. Matsui and H. Satz. This prediction is based on the idea that in the plasma phase the interaction potential is expected to be screened beyond the Debye length. This will prevent $c\bar{c}$ states with a radius greater than the Debye length, such as the J/Psi resonance, from forming. Observations of the suppression by the NA50 experiment are shown in Figure 7. In Figure 7a is shown the J/Ψ production normalized to the Drell-Yan yield, compared to calculations of the suppression expected in nuclear matter. In Figure 7b is plotted the ratio of measured to expected J/Ψ suppression. For higher energy densities an anomalously large suppression is observed as is expected from charmonium melting in a QGP.

The PHENIX collaboration at RHIC also observed a significant J/Ψ suppression in central Au-Au collisions. They have shown that the J/Ψ suppression at these higher energies is indeed larger than that expected from a extrapolating of cold nuclear matter effects as measured in d-Au collisions. Contrary to expectations the suppression at RHIC is found to be similar to that observed at the SPS. The models that described the J/Ψ suppression at the SPS all predicted a significantly larger suppression at RHIC. At these RHIC energies however, central collisions produce multiple pairs of heavy quarks. These multiple c and $\bar{c}$ quarks, originally produced in separate incoherent interactions, might coalesce and form a J/Ψ. This additional production mechanism complicates the interpretation, and can at RHIC be responsible for some re-

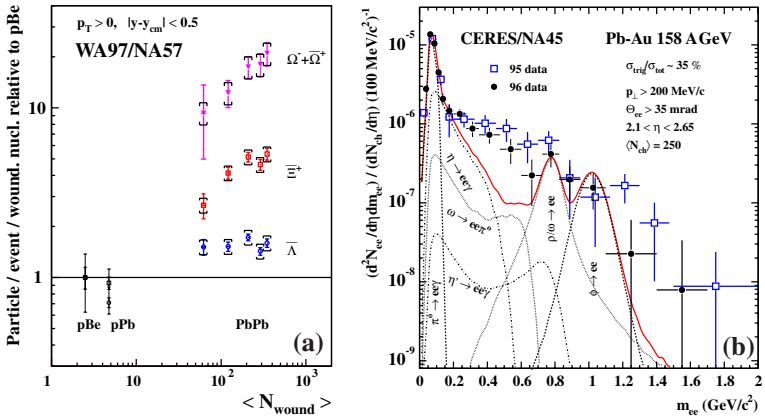

Figure 8. *a) Strangeness enhancements measured by the NA57 experiment. The enhancements are defined as the particle yields normalized by the number of participating nucleons in the collision, and divided by the observed yield in proton-beryllium collisions. The yields expected from a simple superposition of nucleon-nucleon collisions would then lie on a straight line positioned at unity. b) Normalized invariant-mass spectra of dilepton pairs. The measured yield is compared to the known hadronic decay sources, showing the individual contributions. At low invariant-mass a clear excess of the dilepton yield is observed*

generation of the J/Ψ yield. At LHC energies this production mechanism could actually become so important that there is no longer a J/Ψ suppression but instead a J/Ψ enhancement. This would be an unambiguous signature of quark coalesence.

3.1.4 Strangeness production

Strange particles produced in heavy-ion collisions give important information on the collision mechanism. In particular, if a phase transition to a QGP state takes place, one would expect an enhancement in the yields of strange and multi-strange particles in nucleus-nucleus reactions compared to those from proton-nucleus interactions. In fact, the formation of such a state will lead to equilibration of strange quarks on a time scale of a few fm/c, and to the formation of multi-strange baryons and antibaryons close to thermal and chemical hadronic equilibrium. Their abundances will be frozen at the critical temperature T_c since hadronic reactions are too slow to compete with the rapid collective expansion of the fireball at temperatures below T_c. It is expected that the enhancement should be more pronounced for multi-strange than for singly strange particles. The experimental results on Λ, Ξ and Ω from the WA97/NA57 collaboration are plotted in Figure 8a and indeed show this predicted enhancement. However, the NA49 collaboration has found

that this enhancement is already present in small colliding systems e.g. Si-Si collisions. Since QGP formation in such small systems is perhaps less likely. An alternative enhancement mechanism could be the reduction of canonical suppression in an extended system.

3.1.5 Dileptons

Correlated electron-positron pairs (dileptons) provide a probe of the expanding system at an early stage. The absence of any final state interaction conserves the primary information within the limits imposed by the space-time folding over the emission period. In the low-mass region, the thermal radiation is dominated by the decays of the light vector mesons ρ, ω, and ϕ. The ρ is of particular interest, due to its short lifetime of 1.3 fm/c, therefore its in-medium behavior around the critical temperature provides a direct link to chiral symmetry restoration. The shape of the measured dilepton yield by NA45/CERES, as shown in Figure 8b, can be explained by a strong medium modification of the intermediate ρ. This modification can theoretically be described by a reduction in mass (as a precursor of chiral symmetry restoration), known as Brown-Rho scaling, or by a spreading of the width in a hadronic medium. More recent experimental results from the NA60 collaboration, with much improved accuracy, show that the space-time averaged ρ spectral function is strongly broadened, but not shifted in mass.

3.1.6 Particle yields

The measurement of the integrated yields of the various hadron species produced in the collisions (chemical composition) provides information on the chemical freeze-out temperature and baryon chemical potential. These two parameters are obtained from a fitting a thermal model to the yields. In Figure 9a the yields measured at RHIC are compared to those obtained from a the fit to the thermal model, where all the particles yields are characterized by a single chemical freeze-out temperature of 164 MeV and a single baryon chemical potential of 30 MeV. This freeze-out temperature is very close to the critical temperature predicted by lattice QCD calculations.

The statistical description of the hadron yields is not only successful for heavy-ion collisions at RHIC energies but also at lower energies. This allows us to plot the chemical freeze-out temperature versus μ_B obtained at different energies in a phase diagram (see Figure 9b). It is seen that at chemical potentials of less than about 400 MeV, the temperatures trace the phase boundary predicted by lattice QCD (dashed curve in Figure 9b). This observation of a limiting temperature is considered to be a strong indication that the relevant degrees of freedom have changed from that of hadronic matter.

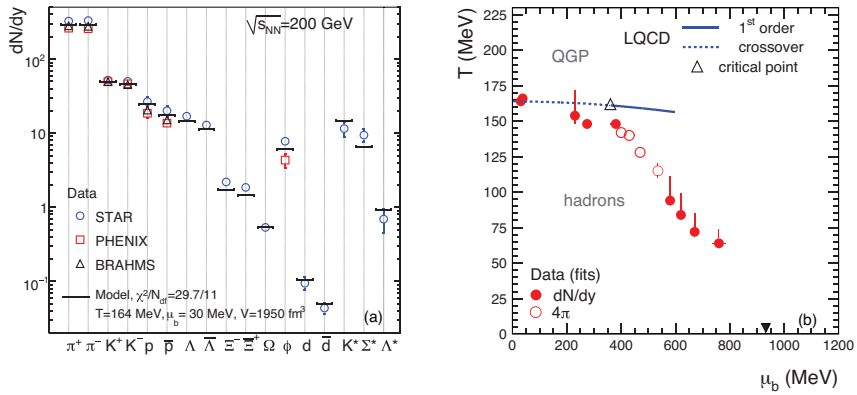

Figure 9. *a) The measured hadron yields at RHIC compared to the best fit from a thermal model. b) The phase diagram of QCD matter in the $T - \mu_B$ plane. The full and open symbols show the obtained chemical freeze-out temperature and μ_B obtained from fitting the thermal model to the measured hadron yields. A lattice QCD estimate of the location of the critical point is indicated by the open triangle. The dashed and full line represent the lattice QCD prediction for the crossover and first order phase transition from a QGP to a hadron gas, respectively.*

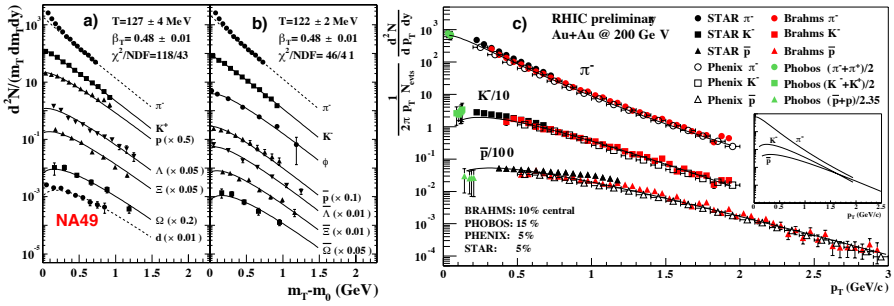

Figure 10. *NA49 (SPS) and RHIC low-p_t spectra. (a) and (b) shows the transverse momentum measured by NA49 at $\sqrt{s_{NN}} = 17$ GeV . The lines are a fit of a hydrodynamic model to the transverse momentum spectra. (c) shows the transverse momenta measured at RHIC.*

3.1.7 Spectra

The particle spectra provide much more information than the integrated particle yields alone. The particle yields as a function of transverse momentum reveal the dynamics of the collision, characterized by the temperature and transverse flow velocity of the system at freeze-out. The kinetic freeze-out

corresponds to the final stage of the collision when the system becomes so dilute that all interactions between the particles cease to exist so that the momentum distributions do not change anymore. Figure 10a and b show the transverse momentum distributions at $\sqrt{s_{\rm NN}} = 17$ GeV from NA49. The lines are a fit to the particle spectra with a hydrodynamically inspired model (blast wave). The fit describes all the particle spectra rather well which shows that these spectra can be characterized by the two parameters of the model: a single kinetic freeze-out temperature and a common transverse flow velocity. Figure 10c shows the combined pion, Kaon and proton $p_{\rm t}$-spectra from the four RHIC experiments. Also at these energies, a common fit to all the spectra shows that the system seems to freeze-out with a temperature and with a transverse flow velocity similar to that observed at SPS energies.

3.1.8 Anisotropic flow

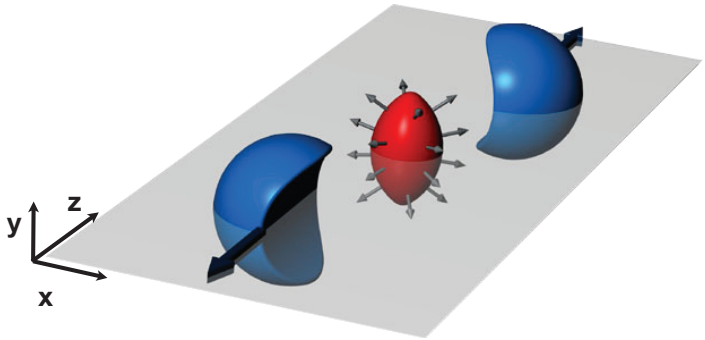

Figure 11. *Almond shaped interaction volume after a non-central collision of two nuclei. The spatial anisotropy with respect to the x-z plane (reaction plane) translates into a momentum anisotropy of the particles produced in the collision (anisotropic flow).*

Flow is an ever-present phenomenon in nucleus–nucleus collisions, from low-energy fixed-target reactions up to $\sqrt{s_{\rm NN}} = 200$ GeV collisions at the Relativistic Heavy Ion Collider (RHIC), and is expected to be observed at the Large Hadron Collider (LHC). Flow signals the presence of multiple interactions between the constituents and is an unavoidable consequence of thermalization.

The usual theoretical tools used to describe flow are hydrodynamic or microscopic transport (cascade) calculations. Flow depends in the transport models on the opacity, be it partonic or hadronic. Hydrodynamics becomes valid when the mean free path of particles is much smaller than the system size and allows for a description of the system in terms of macroscopic quantities. This can be used to determine the equation of state of the flowing matter

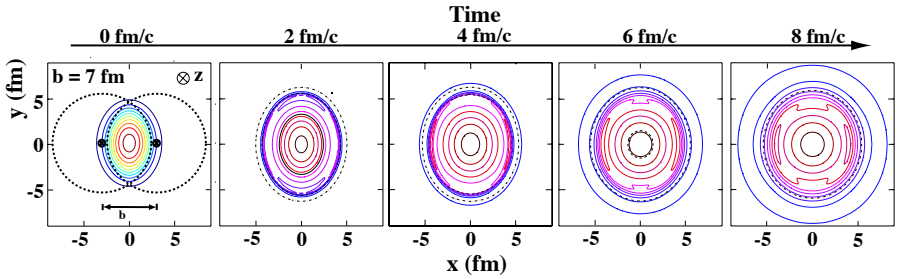

Figure 12. *The created initial transverse energy density profile and its time dependence in coordinate space for a non-central heavy-ion collision. The z-axis is along the colliding beams, the x-axis is defined by the impact parameter* **b** *(the vector connecting the centers of the colliding heavy-ions, perpendicular to the beam axis).*

and, in particular, on the value of the sound velocity, which is a measure the magnitude of the collective flow. In both types of models it may be possible to deduce from a flow measurement whether the flow originates from partonic or hadronic matter or from the hadronization process.

Experimentally the most direct evidence of flow comes from the observation of anisotropic flow, which is the anisotropy in the particle momentum distributions correlated with the reaction plane. A sketch of a heavy ion collision is shown in Figure 11. The reaction plane is defined by the impact parameter, x, and the beam direction z. The resulting spatial anisotropy with respect to the reaction plane translates into a momentum anisotropy of the particles produced in the collision. The energy density profile and the its evolution with time in a non-central collision is shown in Figure 12.

A convenient way of characterizing the various patterns of anisotropic flow is to use a Fourier expansion of the triple differential invariant distributions:

$$E\frac{\mathrm{d}^3N}{\mathrm{d}^3\mathbf{p}} = \frac{1}{2\pi}\frac{\mathrm{d}^2N}{p_\mathrm{t}\mathrm{d}p_\mathrm{t},\mathrm{d}y}\left\{1+2\sum_{n=1}^{+\infty}v_n\cos[n(\varphi-\Psi_R)]\right\},$$

where φ and Ψ_R are the azimuthal angles of a particle produced in the collision and the reaction-plane , respectively. The sine terms in such an expansion vanish due to reflection symmetry with respect to the reaction plane. The Fourier coefficients are given by

$$v_n(p_\mathrm{t},y) = \langle\cos[n(\varphi-\Psi_R)]\rangle,$$

where the angular brackets denote an average over the particles, summed over all events, in the (p_t,y) bin under study. In this parameterization, the first two coefficients, v_1 and v_2, are known as directed and elliptic flow, respectively.

Figure 13 shows the measured dependence of v_2 as a function of the center-of-mass energy. From this figure it is seen that a positive v_2 measured at low

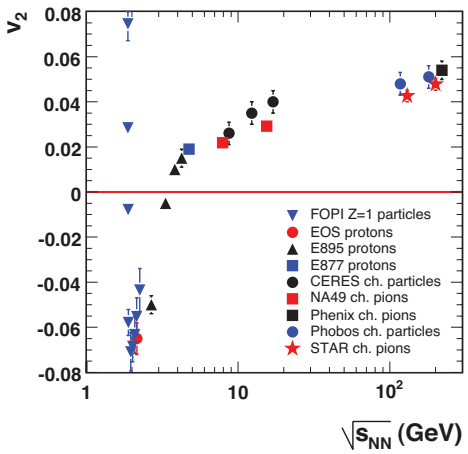

Figure 13. *Elliptic flow at midrapidity as function of beam energy.*

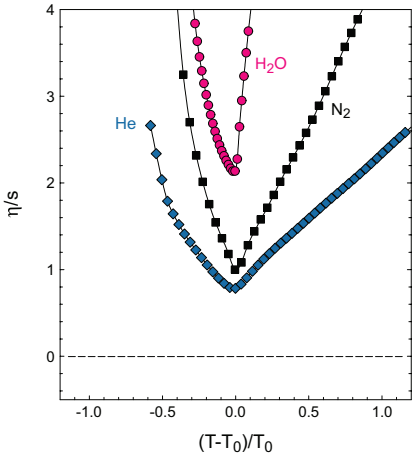

Figure 14. *The ratio η/s versus temperature for several liquids.*

energies becomes negative and reaches its lowest value at about 2 GeV. Above this energy v_2 rises again to positive values. The positive v_2 at lower energies reflects the bounce-off of the two colliding heavy ions that subsequently fragment in the reaction plane. At these energies, beam rapidity and mid-rapidity have significant overlap. As the energy increases, particle emission from the strongly compressed matter in the center of the collision is shadowed by the passing spectator nucleons. This causes the particles produced to emerge perpendicular to the reaction plane leading to a negative value of v_2 (squeeze-out). At top AGS and SPS energies, due to Lorentz contraction, the timescale for the spectator nucleons to pass the created hot and dense system becomes much shorter than the characteristic time for the buildup of transverse flow. At these energies the elliptic flow becomes in-plane again (positive v_2) with a magnitude that is proportional to the initial spatial anisotropy of the created system and the sound velocity in the medium.

The large elliptic flow measured at RHIC is surprisingly well described by ideal hydrodynamics, which applies to fluids that are in thermal equilibrium and have no viscosity, a perfect fluid. The reason for this perfect fluid behavior of the matter created at RHIC energies is not fully understood. It may indicate that it is a strongly coupled QGP, or a state of matter with as yet unknown properties.

Viscous hydrodynamical models were recently developed to investigate to what extent the matter created at RHIC is indeed a perfect fluid. Here the quantity of interest is the ratio of the shear viscosity η to the entropy density s (this ratio is inversely proportional to the Reynolds number). Figure 14 shows the value of η/s versus temperature for different liquids. Water close to the triple point reaches a value of $\eta/s = 2$, while for liquid helium the

ratio is as low as $\eta/s = 0.7$. This raises the more fundamental question: is there is a lower bound that can be derived from first principles on how perfect a liquid can be? Such a bound has been obtained by Kovtun, Son and Starinets, who showed that conformal field theories with gravity duals (anti-de Sitter/Conformal Field Theory) yield a ratio of $\eta/s = 1/4\pi$ (in natural units). They conjectured that this value is a lower bound for any relativistic thermal field theory.

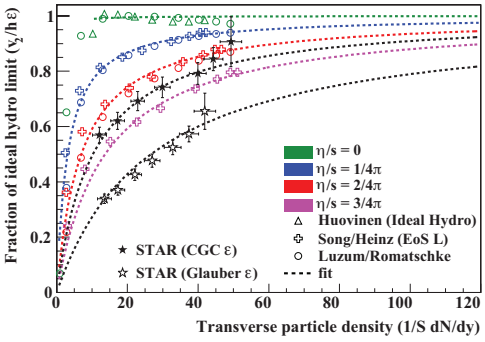

Figure 15. *Elliptic flow v_2 normalized to the spatial eccentricity ε and the limit of this ratio derived from ideal hydro h versus the transverse particle density. The full and open stars are derived from elliptic flow measurements by STAR.*

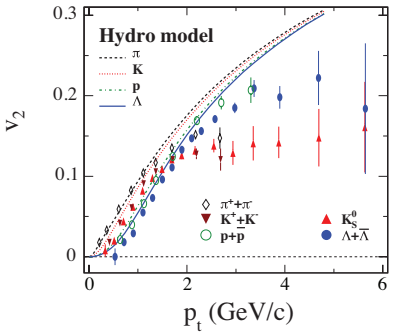

Figure 16. *Elliptic flow for various particle types as function of transverse momentum.*

Figure 15 shows elliptic flow, divided by the spatial eccentricity of the created system (ε), normalized to the ideal hydro limit (h) as a function of the transverse particle density. The open colored symbols are theoretical calculations with different values of η/s. The figure clearly shows that even small shear viscosities, of the order of the bound, already significantly reduce the elliptic flow. Also plotted in Figure 15 are data on elliptic flow from STAR that show a reduction which is compatible with an η/s of a few times the bound. However, the comparison between data and theory depends intimately on the equation of state and the value of the spatial eccentricity, both of which are poorly known for the data obtained at RHIC. For instance, the data would indicate a value of $\eta/s < 3/4\pi$, assuming a soft equation of state and Color Glass Condensate initial conditions (full stars in Figure 15). On the other hand, a larger value of η/s is obtained when a hard equation of state and Glauber wounded nucleon initial conditions are assumed (open stars). These estimates of η/s include possible contributions from the pre-equilibrium phase and from the hadronic phase. Therefore they can be considered to be upper limits on η/s in the QGP phase.

The measurement of elliptic flow as function of transverse momentum provides more detailed constraints on the properties of the system at kinetic

freeze-out, in addition to the information obtained from hadron spectra. Figure 16 compares the measured elliptic flow of various particle species as function of transverse momentum with that from ideal hydrodynamical calculations. At low transverse momenta the strong characteristic mass dependence of elliptic flow is rather well described by ideal hydrodynamics. This description can be improved by introducing a non-zero viscosity via a hybrid description of ideal hydrodynamics and a hadronic cascade model (not shown). The good agreement between the measured integrated and differential elliptic flow and these theoretical descriptions lends strong support to the underlying assumption that the system is partonic and is approaching thermalization at the early stage of the collision.

The particle dependence of v_2 at higher transverse momenta falls, within uncertainties, into two distinct classes: that of baryons and that of mesons. In the proposed scenario of constituent quark coalescence the mesons (baryons) carry twice (three times) the constituent quark v_2 which naturally leads to the observed baryon/meson scaling. This observation may indicate that the flow of partonic degrees of freedom is observed.

3.1.9 Jet quenching

The products of initial state hard scatterings, e.g. mesons containing charm or bottom, high-p_t photons and high-p_t hadrons provide a detailed probe of the created system. While initial state production of these probes is relatively unaffected by the presence of the created system it was predicted that partons would lose energy while traversing the system, mainly by induced gluon radiation. The amount of energy loss in this picture is directly related to the parton density. Thus by studying these high-p_t probes the density of the created system can be determined. In heavy-ion collisions at RHIC, jets with transverse energies above 40 GeV are produced in abundance, however the abundant soft particle production in heavy-ion collisions tends to obscure the characteristic jet structures. At sufficient high-p_t the contribution from the tails of the soft particle production becomes negligible and jets can be identified by their leading particles. When the parton loses energy, the hadrons into which it fragments will, on average, have lower transverse momenta. Therefore the parton energy loss leads to a suppression of the yield of high-p_t hadrons compared to nucleon-nucleon collisions where there is no dense medium. One of the observables suggested for measuring energy loss is the so called nuclear modification factor defined by

$$R_{\mathrm{AA}}(p_t) = \frac{\mathrm{d}^2\sigma_{\mathrm{AA}}/\mathrm{d}y\mathrm{d}p_t}{\langle N_{\mathrm{binary}}\rangle \mathrm{d}^2\sigma_{\mathrm{pp}}/\mathrm{d}y\mathrm{d}p_t},$$

where $\mathrm{d}^2\sigma_{\mathrm{pp}}/\mathrm{d}y\mathrm{d}p_t$ is the inclusive cross section measured in p+p collisions and $\langle N_{\mathrm{binary}}\rangle$ accounts for the geometrical scaling from p+p to nuclear collisions. In the case that a Au+Au collision is an incoherent superposition of p+p collisions this ratio R_{AA} would be unity. Energy loss and shadowing

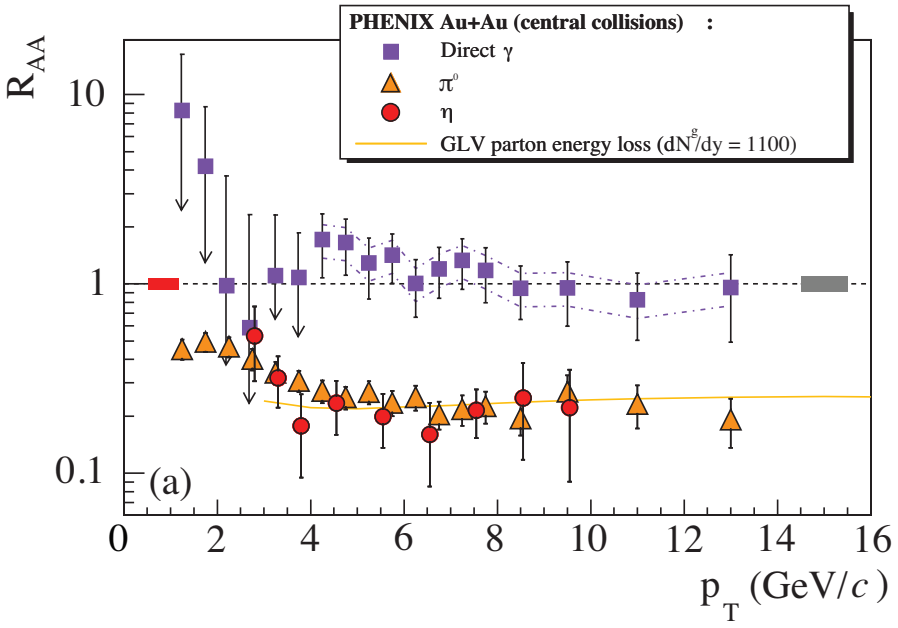

Figure 17. *The nuclear modification factor $R_{\rm AA}$ as function of transverse momentum for π_0's, η's and direct photons.*

would reduce this ratio below unity while anti-shadowing and the Cronin effect would lead to a value above unity. Figure 17a shows this ratio for π_0's and η's in central Au+Au collisions at mid-rapidity. The ratio is well below one and at high-p_t the suppression is about a factor of 5. In the same figure the $R_{\rm AA}$ for direct photons is shown. Direct photons do not couple via the strong force with the produced system and therefore, as expected, their $R_{\rm AA}$ at high-p_t is compatible with unity.

The parton energy loss shows up even more dramatically in the azimuthal correlations as shown in Figure 18b. Azimuthal correlations between two high-p_t hadrons in a nucleon-nucleon collision exhibit strong peaks at 0 and π because the two partons from a hard collision traverse the system back to back in azimuth. In the dense medium created in heavy-ion collisions the energy loss reduces the yield of high-p_t particles; therefore the high-p_t particles which do escape the system are on average produced close to the surface. The recoiling associated parton is maximally affected by the energy loss causing a suppression of the away-side hadron jet. This jet-quenching effect is clearly observed in the gold-gold measurements shown in Figure **??**b.

The magnitude of the observed suppression at the top RHIC energy indicates, in the jet quenching picture, densities which are at least a factor 30 higher than in nuclear matter. To become more quantitative the energy loss

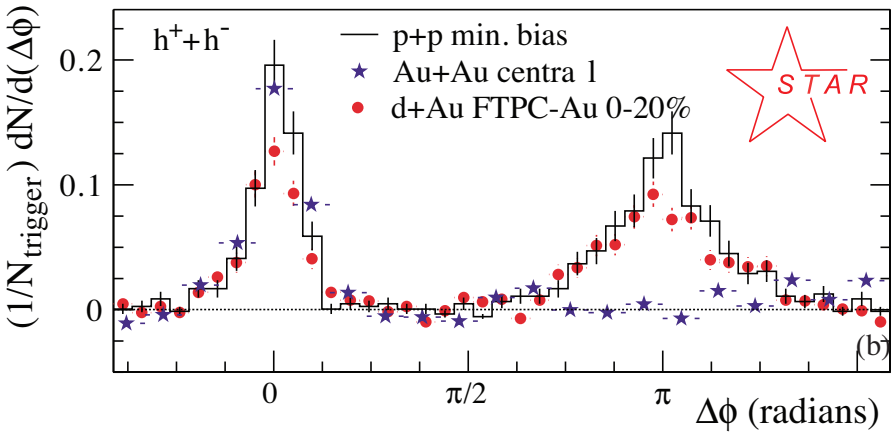

Figure 18. *Measured back to back leading hadron azimuthal correlations.*

mechanism and the response of the medium has to be understood in more detail.

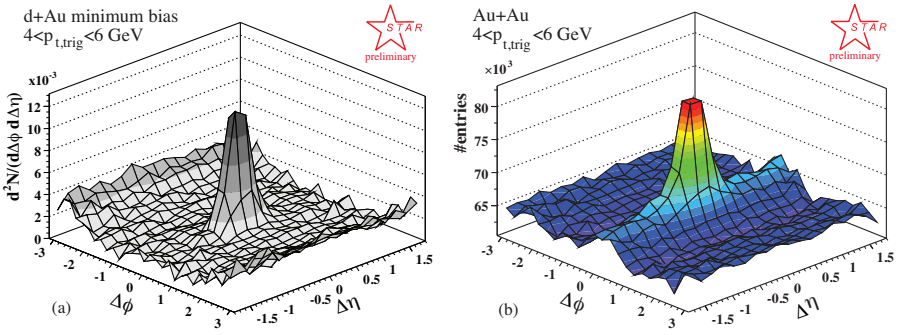

Figure 19. *Preliminary di-hadron correlations in $\Delta\eta$ and $\Delta\phi$ for a) d+Au and b) Au+Au. The trigger particle is between $4 < p_t < 6$ GeV/c and the associated particles are between 2 GeV/c $< p_t < p_t^{trig}$.*

One recent striking result, which might provide additional information on the response of the medium, is the di-hadron correlation at intermediate p_t. The di-hadron correlation, in azimuth and in pseudo-rapidity η, shows that the near-side correlation (small $\Delta\phi$ which was already shown in Figure **??**b) extends over large $\Delta\eta$. Figure 19 shows this correlation for d+Au and Au+Au collisions. It is clear that this longe range $\Delta\eta$ correlation is unique for heavy-ion collisions. The long range correlation is approximately independent of $\Delta\eta$ and is therefore referred to as *the ridge*.

4 Heavy-Ions at the LHC

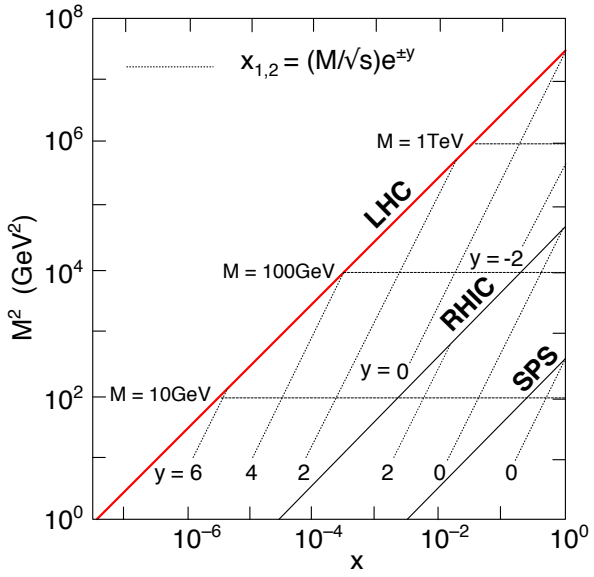

Figure 20. *The range of Bjorken $x_{1,2}$ and M^2, relevant for particle production in nucleus-nucleus collisions at the top SPS ($\sqrt{s_{NN}} = 17.2$ GeV), RHIC ($\sqrt{s_{NN}} = 200$ GeV) and LHC ($\sqrt{s_{NN}} = 5.5$ TeV) energies.*

The LHC at CERN will provide colliding Pb ions with an energy of $\sqrt{s_{NN}} = 5.5$ TeV. This exceeds the maximum energy of 200 GeV available at RHIC by a factor 30 and will open up a new physics domain. Qualitative new features of the heavy-ion collisions at the LHC include:

- Particle production is determined by high-density saturated parton distributions.

  The LHC heavy-ion program accesses a novel range of low Bjorken-x values (see Figure 20), where strong nuclear shadowing is expected. The initial density of gluons is expected to be close to saturation of the available phase space. These very high initial densities allow to describe important aspects of the subsequent time evolution in terms of classical chromodynamics. The ALICE detector will probe a continuous range of x as low as $\sim 10^{-5}$.

- Hard processes become abundant.

  The abundance of hard processes at the LHC will allow for precision test of perturbative QCD. In addition, the large jet rates at the LHC permit detailed measurements of jet quenching to study the early stages of the collision.

- Access to weakly interacting hard probes.

  Direct photons as well as Z^0 and $W^{\pm}$ bosons produced in hard processes will provide information about nuclear parton distributions at high Q^2. Jet tagging with such probes yields a calibrated energy scale for jet quenching studies.

- Fireball expansion is dominated by parton dynamics.

  Due to the expected longer lifetime of the QGP, the parton dynamics will dominate over the hadronic contribution to the fireball expansion and therefore collective features such as elliptic flow provide much stronger constraints on the EoS of the partonic phase.

Of course, the large increase in center of mass energy provided by the LHC will offer unique opportunities for new and unexpected discoveries.

It is expected that the LHC can deliver luminosities of 10^{27} cm^2 s^{-1} for Pb-Pb collisions, which results in a minimum-bias interaction rate of 8 kHz. Lighter ions can be delivered with higher luminosities of up to 10^{29} cm^2 s^{-1}, corresponding to an interaction rate of several 100 kHz.

5 The ALICE Detector

At the LHC three collaborations (ALICE, ATLAS and CMS) have a heavy-ion program. The ALICE collaboration has designed a detector optimized for heavy-ion collisions. The apparatus will detect and identify hadrons, leptons and photons over a wide range of momenta. The requirement to study the various probes of interest in a very high multiplicity environment, which may be as large as 8 000 charged particles per unit of rapidity in central Pb-Pb collisions, imposes severe demands on the tracking of charged particles. A schematic view of the ALICE detector is shown in Figure 21. Figure 22 shows the particle tracks originating from a single heavy-ion collision in the ALICE detector.

In ALICE, the excellent PID capabilities, momentum resolution and complete azimuthal coverage of the central detectors allow comprehensive measurements of particle ratios, momentum spectra, particle correlations, anisotropic flow and event-by-event fluctuations. These observables do not require large amounts of data and will either quickly confirm our current understanding of high density QCD or provide fundamental new insights.

The LHC will be the first machine where heavy quarks are produced abundantly in heavy-ion collisions. Due to the excellent impact parameter resolution and particle identification capabilities, ALICE is well suited to study charm and beauty. From detailed simulation studies of the benchmark channel $\mathrm{D}^0 \to \mathrm{K}^-\pi^+$ it is found that in one LHC year at nominal luminosity, we cover the transverse momentum range $1 < p_\mathrm{t} < 18$ GeV/c in the central barrel acceptance of $|\eta| < 0.9$. Beauty production can be measured from semi-leptonic

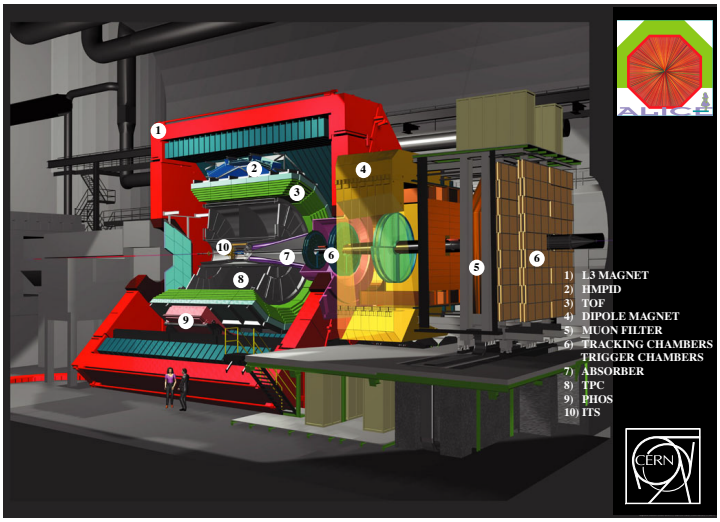

Figure 21. *The ALICE detector layout*

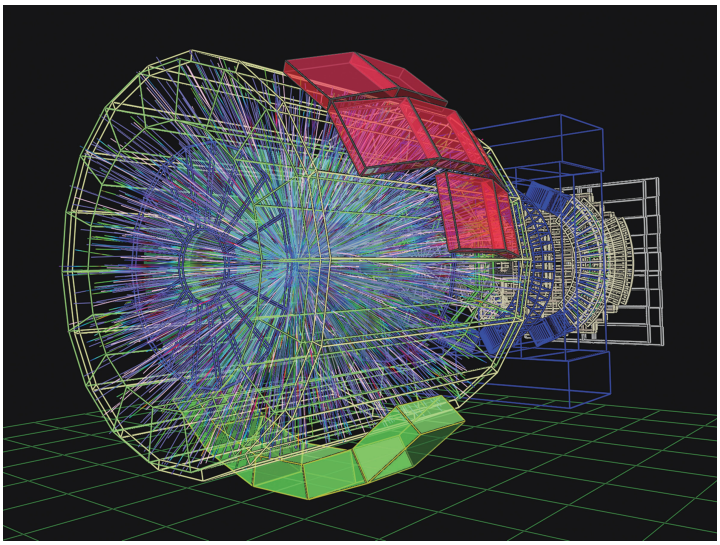

Figure 22. *Particle tracks from a single simulated heavy-ion collision in ALICE*

decays in the range of $2 < p_{\mathrm{t}} < 30$ GeV/c. Single muons and opposite-sign dimuon pairs detected in the muon spectrometer allow for measurements of open-beauty production with high statistics in the pseudorapidity region $-4 < \eta < -2.5$. The measurement of heavy flavor production down to very low transverse momenta is sensitive to the collective motion of heavy quarks

in the medium and will provide strong constraints on the thermalization of light quarks. At higher momenta, on the other hand, the measurement of heavy flavor production will provide detailed information on the energy loss mechanism.

In addition to open charm and open beauty, the complete spectrum of heavy quarkonia states (J/Ψ, Ψ', Υ, Υ' and Υ") is accessible at the LHC. In ALICE quarkonia are detected at mid-rapidity ($-0.9 < \eta < 0.9$) in the dielectron channel, and at ($-4.0 < \eta < -2.5$) in the dimuon channel, which will allow for detailed studies of suppression effects due to deconfinement.

The jet rates in central Pb-Pb collisions at the LHC in the ALICE acceptance are sufficient to map out the energy dependence of jet fragmentation over a wide kinematic range up to $E_{\rm t} \simeq 200$ GeV. Jet reconstruction in nuclear collisions has to cope with the large background from the underlying event, therefore, jet reconstruction has to be limited to a small cone of fixed radius in azimuth and pseudorapidity ranging between 0.3 – 0.5. In addition, a transverse momentum cut in the range 1–2 GeV/c has to be applied to reduce the background. As a consequence, even for perfect calorimetry, the transverse energy resolution is limited to $\simeq 20\%$. Another very promising approach to study jet fragmentation is using prompt photons to tag charged jets emitted in the opposite direction. Prompt photons allow the study of the hard interaction without any final state modifications and with this tag the in-medium modification of the fragmentation function will be measured with an accuracy of the order of a few percent. The combined tracking capabilities of the ALICE detector combined with electromagnetic calorimetry represent an ideal tool for jet structure modifications at the LHC.

6 Summary

The relativistic heavy-ion collision program provides a unique tool to test the phase diagram of strongly interacting matter under controlled conditions. The program so far has tremendously improved our understanding of the probes and we start to quantitatively characterize the created system. The heavy-ion program at the LHC will allow for a more precise characterization of the QGP and will allow us to explore new aspects of the structure of strongly interacting nuclear matter. With the LHC machine currently delivering the first proton proton collisions and its detectors fully operational we are looking forward to the first heavy-ion collisions.

Acknowledgments

I would like to thank the organizers of the school for their hospitality and creating this wonderful stimulating environment. I would also like to thank M. Botje for his help with preparing this document.

Bibliography

[1] R. Stock, "Relativistic Nucleus-Nucleus Collisions and the QCD Matter Phase Diagram," arXiv:0807.1610 [nucl-ex].

[2] H. Satz, "The States of Matter in QCD," arXiv:0903.2778 [hep-ph].

[3] F. Karsch and E. Laermann. Thermodynamics and in-medium hadron properties from lattice QCD. In R.C. Hwa, editor, *Quark gluon plasma*, pages 1–59. 2003.

[4] P. Braun-Munzinger and J. Stachel, "Charmonium from Statistical Hadronization of Heavy Quarks – a Probe for Deconfinement in the Quark-Gluon Plasma," arXiv:0901.2500 [nucl-th].

[5] H. Oeschler, H. G. Ritter and N. Xu, arXiv:0908.1771 [nucl-ex].

[6] U. W. Heinz, "Early collective expansion: Relativistic hydrodynamics and the transport properties of QCD matter," arXiv:0901.4355 [nucl-th].

[7] S. A. Voloshin, A. M. Poskanzer and R. Snellings, "Collective phenomena in non-central nuclear collisions," arXiv:0809.2949 [nucl-ex].

[8] R. Rapp and H. van Hees, "Heavy Quarks in the Quark-Gluon Plasma," arXiv:0903.1096 [hep-ph].

[9] U. A. Wiedemann, "Jet Quenching in Heavy Ion Collisions," arXiv:0908.2306 [hep-ph].